



Lithium ferrite: The study on magnetic and complex permittivity characteristics

Madhavaprasad Dasari^{1,*}, Ganapathi Rao Gajula², Daruvuru Hanumantha Rao¹,
Arun Kumar Chintabathini², Samatha Kurimella², Bharadwaj Somayajula¹

¹Department of Physics, GITAM Institute of Technology, GITAM University, Visakhapatnam – 45, Andhra Pradesh, India

²Department of Physics, Andhra University, Visakhapatnam – 530003, Andhra Pradesh, India

Received 12 September 2016; Received in revised 16 November 2016; Received in revised form 24 December 2016;
Accepted 2 January 2017

Abstract

Lithium ferrite ($\text{Li}_{0.5}\text{Fe}_{2.5}\text{O}_4$) powder was prepared by solid state reaction method, which was finally pressed and sintered at 1150°C . The spinel structure of the lithium ferrite was confirmed by X-ray diffraction and grain size estimation was obtained from scanning electron microscope (SEM). Fourier transform infrared spectroscopy (FTIR) confirmed the presence of primary and secondary absorption bands characteristic for spinel structure. The force constants were estimated using absorption bands for the lithium ferrite. Magnetization and dielectric studies were carried out for the sintered sample. Saturation magnetization (M_s) of 59.6 emu/g was achieved and variation of magnetization with temperature was used to identify the Curie temperature. The complex permittivity (ϵ^*) for the lithium ferrite sample was obtained for wide frequency range up to 3 GHz and discussed based on available models. The Curie temperature was estimated around 480°C and verified from both magnetization versus temperature and dielectric constant versus temperature measurements.

Keywords: ferrites, sintering, structural characterization, magnetic and dielectric properties

I. Introduction

Lithium ferrite is commercially available ferrite used in different types of applications, such as: electromagnetic absorbers, fuel cells, sensors and microelectronic materials, due to stability, low conductivity, stress sensitivity and high Curie temperature [1–9]. Spinel ferrites are widely used in high frequency zone operating with Snoek limitation with narrow band width [10–12]. Several preparation methods and different sintering conditions have been used to control chemical composition and structure of lithium ferrite ceramics, as well as to tailor the magnetic and electric properties. The basic method of preparation is still conventional mixing of the corresponding oxides, followed by calcinations and final sintering [13]. The measurement of dielectric and magnetic properties allows understanding of the polarization mechanism of the dipoles [14] associated under the above synthesis and sintering condi-

tions. The measured dielectric and magnetic behaviour could also help understand the dipoles interaction and nonlinear behaviour in lithium ferrite at frequency less than 3 GHz , useful in designing the composite material comprising ferroelectric material [15], microwave devices edge guided isolators and circulators.

In present work, the lithium ferrite was prepared through solid state reaction route and sintered at high temperature. The magnetic and dielectric properties have been studied as a function of temperature and applied field.

II. Experimental procedure

Lithium ferrite ($\text{Li}_{0.5}\text{Fe}_{2.5}\text{O}_4$) powder with the desired composition was prepared using solid state technique. Lithium carbonate (Li_2CO_3) and Fe_2O_3 powders of AR grade were weighted according to the stoichiometric formula of the desired composition:



*Corresponding author: +91 934 881 1777,
fax: +91891275311, e-mail: madhavaprasaddasari@gmail.com

These ingredients were thoroughly mixed in wet atmosphere (methanol) in an agate mortar for 6 h, and then dried by slow evaporation. The mixture was calcined in air for 4 h at 900 °C and again ground. The calcined powder was mixed with the polyvinyl alcohol (PVA), used as a binder, and then pressed into discs with diameter of 1.0 cm and thickness of 1.0–1.5 mm. Finally, the green pellets were sintered at 1150 °C for 4 hours to obtain lithium ferrite (LF) ceramics.

Phase composition of the sintered lithium ferrite was identified using X-ray diffraction (Model: Bruker D8 SSS-CuK α) and grain size was estimated from scanning electron microscope (Model: Carlzeiss Ultra-55). Fourier transform infrared spectroscopy (FTIR) was measured using the Bruker, Germany Model: Vertex 70. Magnetic measurements were carried out at room temperature by applying 20 kOe magnetic field coupled with temperature variation condition using vibrating sample magnetometer (Model: 9T PPMS-Quantum design). The dielectric measurement, such as real part of permittivity and dielectric loss ($\tan \delta$), was carried out using impedance analyser (Model: Agilent technologies model E5062A) for higher frequency range up to 3 GHz at room temperature. The dielectric constant versus temperature measurement at a low frequency (10 kHz) was carried out to understand the polarization mechanism of lithium ferrite. For low frequency measurement of dielectric constant, LCR meter from Wayne Kerr electronics with model number 1J43100 was used.

III. Results and discussion

Figure 1 shows the powder diffraction pattern of the lithium ferrite sample sintered at 1150 °C. The reflection planes of the spinel ferrite structure shown in the X-ray pattern are indexed and compared with standard JCPDF data (89-7832 & 88-06711). Crystal structure was found to be spinel in nature with obtained lattice parameter of $a = 8.3157 \text{ \AA}$, which is in agreement with the previously reported values [16].

The grain structure appears to be uniform in size with the average grain size around 8.3 μm , estimated from

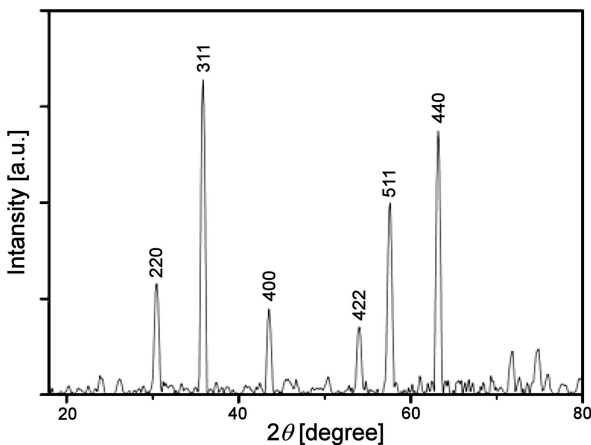


Figure 1. XRD pattern of sintered lithium ferrite sample

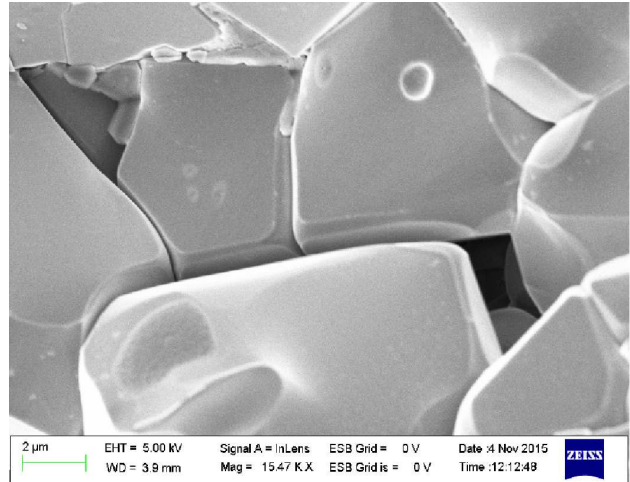


Figure 2. SEM picture of lithium ferrite

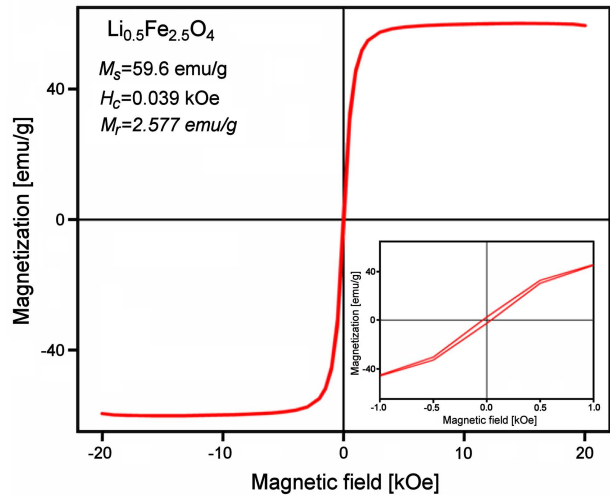


Figure 3. Magnetization variation with the applied magnetic field (H) for lithium ferrite

SEM pictures (Fig. 2). This coarse grain structure could be formed due to the interaction between magnetic particles through agglomeration or coalescence at relatively high sintering temperature. These interactions often lead to diffusion or concentration of dissimilar ions at various sites in the structure leading to higher crystallite size or grain size [17,18]. The discontinuous grain growth hampers the migration of pores to the grain boundary which influences the domain wall contribution in the magnetization mechanism [19,20].

Variation of magnetization with the applied magnetic field (H) for the sintered $\text{Li}_{0.5}\text{Fe}_{2.5}\text{O}_4$ was studied at room temperature. As shown in Fig. 3, magnetization increases with increasing field suggesting movement of the domains or domain boundaries changing direction with respect to applied field. As the applied field increases, the movement of domains or domain walls follows the field at the expense of domains which are unable to orient. This continuous movement of domains leads to the saturation value where domains are completely orientated towards the field. Properties such as

saturation magnetization, coercivity and remanence, determined from measured data, are shown in Fig. 3. The existence of very low coercivity can be observed from the hysteresis (inset in Fig. 3). The saturation magnetization ($M_s = 59.6 \text{ emu/g}$) obtained for the lithium ferrite sample is comparable to the previously reported values [3,5]. The obtained data suggest that the magnetization nature depends on the sub-lattice collinear spin model which depends on the cation distribution in A and B sites. According to Neel this magnetic behaviour is due to the contribution from AB sites rather than AA or BB sites interactions [21]. The net magnetization is a result of difference of sub-lattice magnetization at both (A and B) sites which are coupled through ferromagnetic-nonmagnetic behaviour. Here lithium is expected to be in B sites playing the role of non-magnetic behaviour along with the iron (Fe^{3+}) which is also present in A site. The value of magnetization obtained experimentally is with agreeable range of theoretical value which can be calculated using Bohr magneton [22]. The known magnetic moment calculated for Li^+ ($0 \mu\text{B}$) and Fe^{3+} ($5 \mu\text{B}$) ions could give theoretical value for $\text{Li}_{0.5}\text{Fe}_{2.5}\text{O}_4$ calculated as:

$$\begin{aligned} |M_s|_{theo} &= |M_B| - |M_A| = \\ &= |0.5 \times 0 + 1.5 \times 5|_B \mu_B - |1 \times 5|_A \mu_B \\ |M_s|_{theo} &= 69.82 \text{ A} \cdot \text{m}^2 \cdot \text{kg}^{-1} \end{aligned}$$

The 14% variation between calculated and measured magnetization values could be understood on the basis of the Neel model. The theoretical value is much higher than the experimental one, suggesting the decrease in contribution from B sites to the magnetization. This is perhaps stronger influence than from A sites trending to decrease net magnetization. Reduction of magnetization can only occur when lithium (Li^+) limits the iron mobility during sintering process in B (octahedral) site [23] and these minor changes could also be noticed in the dielectric properties.

Figure 4 shows the temperature variation of magnetization of the lithium ferrite with the Curie temperature at around 480°C . Figure 4 shows the stable nature of magnetization up to the Curie point and fast drop at higher temperature. This variation of magnetization could be due to the complex interaction between lithium and iron ions leading to the spin canting effects in lithium ferrites as reported elsewhere [3,5,24]. This variation of magnetization further depends on the grain size, anisotropy nature, porosity, sintering conditions and cation distribution. Weiss Brillouin theory of ferromagnetism [25] indicates that the magnetic spins experience the thermal stirring at non-zero temperature and internal spin can be reversed by reducing the effective field on either of the sub lattices. These interactions further depend on the distribution of lithium along with iron (Fe^{3+}) ions in B sites and iron (Fe^{3+}) in A sites. This distribution could be further analysed using FTIR

spectroscopy where the occurrence of bands at specific positions indicates the presence of metal ions.

The ferrite has space group $Fd3m\text{-}Oh7$ showing IR bands in the frequency range $400\text{--}1000 \text{ cm}^{-1}$ [26,27] (Fig. 5). Formation of two bands with three subsidiary bands shows the ordered nature of the sample. The broad peak indicates the inverse spinel nature of ferrite due to the distribution of Fe^{3+} in A and B sites [28]. The first band at $\nu_1 = 564.39 \text{ cm}^{-1}$ is related to the stretching vibration of $\text{Fe}^{3+}\text{--O}^{2-}$ in tetrahedral sites along with the subsidiary bands near 661 cm^{-1} and 695 cm^{-1} . The second band at $\nu_2 = 414 \text{ cm}^{-1}$ is related to the metal-oxygen vibration in octahedral sites along with subsidiary band near 496 cm^{-1} . The subsidiary band appearance with additional peak attributed to the presence of two different covalent ions at the tetrahedral sites could only be assigned to $\text{Fe}^{3+}\text{--O}^{2-}$ [29]. Potakova *et al.* [30] suggested the presence of iron (Fe^{2+}) ions in ferrite system producing the splitting of absorption bands which is attributed to the John-Teller distortion inducing deformation. The absorption bands allow calculation of force constants of

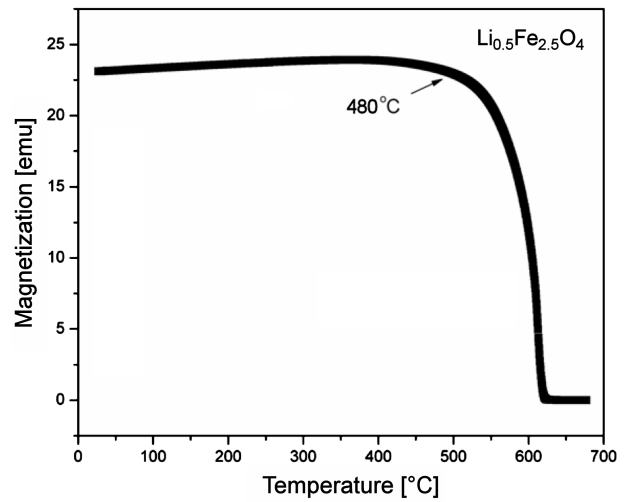


Figure 4. Temperature variation of magnetization of lithium ferrites

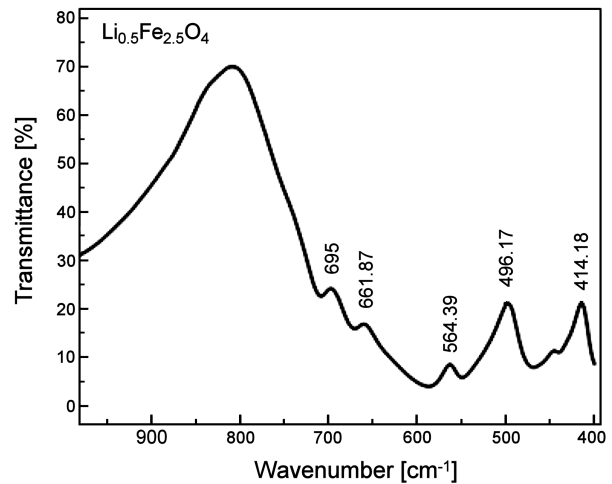


Figure 5. FTIR pattern for lithium ferrite

the ions at the tetrahedral and octahedral sites using the equation [31]:

$$K = 4\pi^2 c^2 \mu \nu^2 \quad (2)$$

where c is the speed of the light ($c = 2.99 \times 10^{10}$ cm/s), ν is the band associated with vibrational frequency for A and B sites, μ is the reduced mass ($\mu = 2.601 \times 10^{-23}$ g). The force constant values obtained for the two main bands are $K_{oct} = 1.57 \times 10^2$ N/m and $K_{tetra} = 2.92 \times 10^2$ N/m. The higher value for the tetrahedral sites suggests higher stretching between these ions leading to the higher force constant than that for the octahedral sites. This leads to assumption of higher value of radii between $Fe^{3+}-O^{2-}$ at tetrahedral sites and reduced value of radii at octahedral sites [32]. The presence of charges at A sites and B sites could be useful in understanding of dielectric nature of the sample.

The complex permittivity was measured using impedance analyser. The real part of permittivity (ϵ') indicates the dielectric capacity or charge storage whereas the loss of energy in material under the applied field is represented by $\tan \delta$. Measurements were carried out in a broad frequency range. Measurements at lower frequencies (Fig. 6) were done indirectly from capacitance, but at higher frequency (Fig. 7) permittivity is measured directly from impedance analyser. In lower frequency range, grain boundaries play more effective role than grains resulting in high permittivity. But, as the frequency increases, jumping frequency of charges cannot match the applied field and therefore do not follow the applied field, reducing the permittivity. In the lithium ferrite the Fe^{2+} ions exist in the octahedral sites and exchanges with Fe^{3+} causing higher resistivity [23]. The presence of Fe^{2+} favours polarization effects reducing the dielectric constant with increase in frequency due to the inability of electrons to hop between Fe^{2+} and Fe^{3+} under applied field. This behaviour of dispersion could be interpreted on the basis of polarization effects determined by local displacements of electrons in the di-

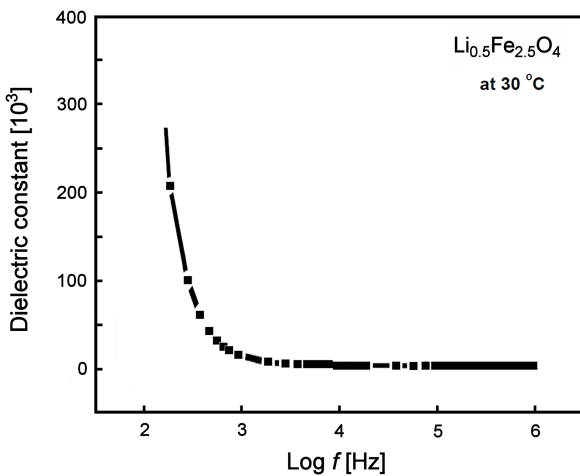


Figure 6. Dielectric constant for lithium ferrite at low frequency

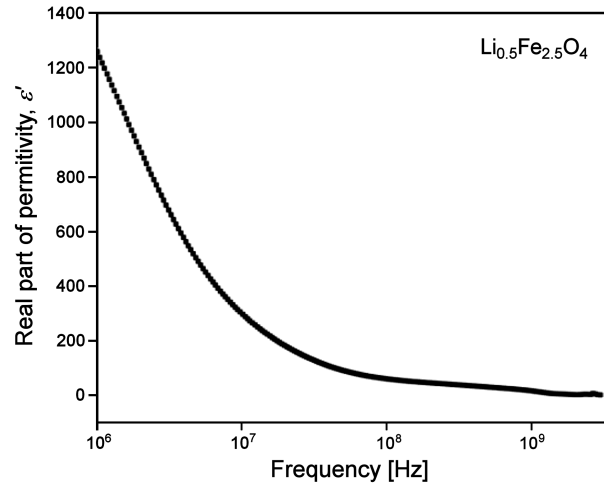


Figure 7. Real part of permittivity for lithium ferrite at high frequency

rection of field in accordance with the Maxwell-Wagner interfacial and Koop's theory [33]. The inability of electrons to polarize under the applied field leads to losses in samples measured as loss tangent for different frequency range.

The loss tangent plotted against frequency shown in Fig. 8 suggests the material characteristic loss at different frequencies. The dispersion in $\tan \delta$ is observed as lag in polarization in the higher frequency. The maximum peak or ferrimagnetic resonance is observed when hopping frequency of electron equals to applied external field which jumping from $Fe^{2+} \longleftrightarrow Fe^{3+}$ expressed as power loss [34]. The loss factor is due to the contribution of resistive nature of the sample mainly from domain wall resonance in grains at lower frequency and spin resonance at high frequency. The broad resonance in multiple regions of the frequency suggests the presence of Fe^{2+}/Fe^{3+} ions in reasonable amounts. The resonances (52.8 MHz and 1.36 GHz, 1.8 GHz) show the jumping probability regions at high frequency for lithium ferrite. Broad peak of loss tangent indicates the

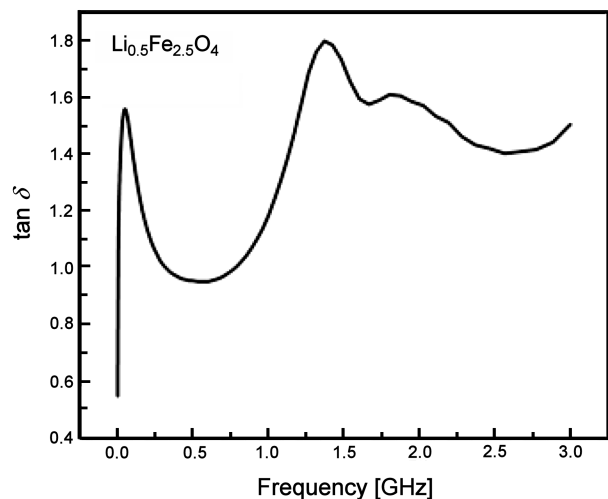


Figure 8. Loss tangent for lithium ferrite at high frequency

presence of distributed relaxation times instead of single one [35]. The maximum dielectric loss in the material can be understood using equation: $\omega \cdot \tau = 1$ where $\omega = 2\pi \cdot f_{max}$ and τ is relaxation time which is jumping probability (p) per unit time. These multiple resonance features could be interpreted based on the loss contribution due to the domains in lower frequency region (MHz) and spin contribution at higher (GHz) frequency region. This is useful in predicting the nature of lithium ferrite at microwave region for absorption purposes.

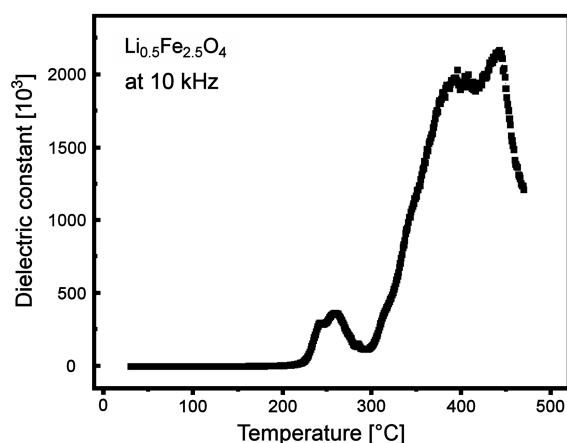


Figure 9. Dielectric constant variation with temperature at 10 kHz

Figure 9 shows the dielectric constant at 10 kHz with increasing temperature for lithium ferrite. Koops suggested that dielectric permittivity is inversely proportional to resistivity nature and increase of permittivity with rise in temperature is expected. Mainly dielectric behaviour at high temperature at low frequency is due to the presence of dipole moments. These dipoles between metallic and oxygen ions may have small separation among them due to the asymmetry in the field. When temperature rises these dipoles increase polarization mechanism creating thermal oscillations and hence dielectric value is high [36,37]. The dielectric constant increases with increase in temperature around 460 °C and beyond this point, the dielectric constant decreases rapidly. The transition point could be further verified from value of Curie temperature obtained from magnetization variation with temperature (Fig. 4), which is in good agreement. This suggests the variation of dielectric constant with temperature could also be due to the magnetic transition where materials change its nature to paramagnetic.

IV. Conclusions

Magnetization and dielectric studies of lithium ferrite sintered at 1150 °C for 4 hours prepared by solid state method are presented in paper. Permittivity decreases with increase in frequency showing the normal polarization behaviour in the sample. Lithium ferrite has saturation magnetization around 59.6 emu/g obtained at room temperature which is well compared with theoretical

value. Magnetization and dielectric variations with temperature show the thermal stability of the lithium ferrite as the Curie temperature around 480 °C is obtained using both techniques. The observation of broad resonance peaks in $\tan \delta$ spectra suggests that the lithium ferrite has multiple jumping probability frequency points in the high frequency zone.

Acknowledgements: Dr. Mukul Gupta and Dr. R J Choudhary of UGC-DAE Consortium for Scientific Research, Indore is gratefully acknowledged for extending the facilities XRD and magnetic measurements respectively.

References

1. A. Goldman, *Modern Ferrite Technology*, Van Nostrand, New York, 1990.
2. R.P. Patil, B.V. Jadhav, M.R. Kadam, D.R. Patil, P.P. Hankare, "LPG gas sensing application of lithium ferrite", *Mater. Focus*, **5** (2016) 46–50.
3. S.S. Bellad, S.C. Watawe, B.K. Chougule, "Microstructure and permeability studies of mixed Li-Cd ferrites", *J. Magn. Magn. Mater.*, **195** (1999) 57–64.
4. M. Bahgat, F.E. Farghaly, S.M. Abdel Basir, O.A. Fouad, "Synthesis, characterization and magnetic properties of microcrystalline lithium cobalt ferrite from spent lithium-ion batteries", *J. Mater. Process. Technol.*, **183** (2007) 117–121.
5. P.P. Hankare, R.P. Patil, U.B. Sankpal, S.D. Jadhav, I.S. Mulla, K.M. Jadhav, B.K. Chougule, "Magnetic and dielectric properties of nanophase manganese-substituted lithium ferrite", *J. Magn. Magn. Mater.*, **321** (2009) 3270–3273.
6. G.M. Argentina, P.D. Baba, "Microwave lithium ferrites: An overview", *IEEE Trans. Microwave Theory Tech.*, **22** (1974) 652–658.
7. R.P. Patil, S.B. Patil, B.V. Jadhav, S.D. Delekar, P.P. Hankare, "Structural and magnetic properties of Co substituted $\text{Li}_{0.5}\text{Fe}_{2.5}\text{O}_4$ ", *J. Magn. Magn. Mater.*, **401** (2016) 870–874.
8. Dipti, P. Kumar, J.K. Juneja, S. Singh, K.K. Raina, C. Prakash, "Improved dielectric and magnetic properties in modified lithium-ferrites", *Ceram. Int.*, **41** (2015) 3293–3297.
9. N. Gupta, C. Mukesh, C. Dimri, S. Kashyap, D.C. Dube, "Processing and properties of cobalt-substituted lithium ferrite in the GHz frequency range", *Ceram. Int.*, **31** (2005) 171–176.
10. M. Sugimoto, "The past, present, and future of ferrites", *J. Am. Ceram. Soc.*, **82** (1999) 269–279.
11. E.F. Kneller, R. Hawig, "The exchange-spring magnet: a new material principle for permanent magnets", *IEEE Trans. Magn.*, **27** (1991) 3588–3560.
12. F. Song, X. Shen, M. Liu, J. Xiang, "Magnetic hard/soft nanocomposite ferrite aligned hollow microfibers and remanence enhancement", *J. Colloid. Interf. Sci.*, **354** (2011) 413–416.
13. M. Tabuchi, K. Ado, H. Kobayashi, I. Matsubara, H. Kageyama, M. Wakits, S. Tsutsui, S. Nasu, Y. Takeda, C. Masquelier, A. Hirano, R. Kanno, "Magnetic properties of metastable lithium iron oxides obtained by solvothermal/hydrothermal reaction", *J. Solid State Chem.*, **141**

- (1998) 554–561.
14. J.R. Macdonald, “Impedance spectroscopy”, *Ann. Biomed. Eng.*, **20** (1992) 289–305.
 15. N. Gupta, S.C. Kashap, D.C. Dube, “Microwave behaviour of substituted lithium ferrite composites in X-band”, *J. Magn. Magn. Mater.*, **288** (2005) 307–314.
 16. S.Y. An, I.-B. Shim, C.S. Kim, “Synthesis and magnetic properties of LiFe_5O_8 powders by a sol-gel process”, *J. Magn. Magn. Mater.*, **290** (2005) 1551–1554.
 17. S.C. Watawe, B.D. Sarwade, S.S. Bellad, B.D. Sutar, B.K. Chaugule, “Microstructure and magnetic properties of Li-Co ferrites”, *J. Mater. Chem. Phys.*, **65** (2000) 173–177.
 18. A. Dhahri, J. Dhahri, S. Zemni, M. Oumezzine, M. Said, H. Vincent, “Synthesis, structural, magnetic and electrical properties of $\text{La}_{1-x}\text{Cd}_x\text{MnO}_3$ manganites ($0.1 \leq x \leq 0.5$)”, *J. Alloys Compds.*, **450** (2008) 12–17.
 19. M.M. Hessien, M.M. Rashad, K. El-Barawy, I.A. Ibrahim, “Influence of manganese substitution and annealing temperature on the formation, microstructure and magnetic properties of Mn-Zn ferrites”, *J. Magn. Magn. Mater.*, **320** (2008) 1615–1621.
 20. O.F. Caltun, L. Spinu, Al. Stancu, L.D. Thung, W. Zhou, “Study of the microstructure and of the permeability spectra of Ni-Zn-Cu ferrites”, *J. Magn. Magn. Mater.*, **242** (2002) 160–162.
 21. B.D. Cullity, *Introduction to Magnetic Materials*, Addison-Wesley, MA, 1972, pp. 141.
 22. R.A. McCurrie I, *Ferromagnetic Materials: Structures and Properties*, Academic Press, San Diego, 1994, pp. 132.
 23. S.S. Bellad, R.B. Pujar, B.K. Chougule, “Structural and magnetic properties of some mixed Li-Cd ferrites”, *Mater. Chem. Phys.*, **52** (1998) 166–169.
 24. L. Dormann, A. Tomas, M. Nogués, “Cation ordering in LiFe_5O_8 studied by Mössbauer spectroscopy and X-ray crystallography”, *Phys. Status Solidi A*, **77** (1983) 611–618.
 25. S. Krupicka, P. Novak, *Ferromagnetic Materials: A Handbook on the Properties of Magnetically Ordered Substances*, edited by E.P. Wohlfarth, Vol. 3, Ed. E.P. Wohlfarth, North-Holland, Amsterdam (1982) pp. 189.
 26. W.B. White, B.A. De Angelis, “Interpretation of the vibrational spectra of spinels”, *Spectrochim Acta A*, **23** (1967) 985–995.
 27. R.D. Waldron, “Infrared spectra of ferrites”, *Phys. Rev.*, **99** (1955) 1727–1735.
 28. J. Smit, H.P.J. Wijn, *Ferrites*, Philips Technical library, Wiley, New York (1959).
 29. N.M. Deraz, “Fabrication, characterization and magnetic behaviour of alumina-doped zinc ferrite nano-particles”, *J. Anal. Appl. Pyrol.*, **91** (2011) 48–54.
 30. V.A. Potakova, N.D. Zverv, V.P. Romanov, “On the cation distribution in $\text{Ni}_{1-x-y}\text{Fe}_x^{2+}\text{Zn}_y\text{Fe}_2^{3+}\text{O}_4$ spinel ferrites”, *Phys. Status Solidi A*, **12** (1972) 623–627.
 31. P.A. Shaikh, R.C. Kambale, A.V. Rao, Y.D. Kolekar, “Structural, magnetic and electrical properties of Co-Ni-Mn ferrites synthesized by co-precipitation method”, *J. Alloys Compd.*, **492** (2010) 590–596.
 32. H.M. Zaki, H.A. Dawoud, “Far-infrared spectra for copper-zinc mixed ferrites”, *Physica B*, **405** (2010) 4476–4479.
 33. C.G. Koops, “On the dispersion of resistivity and dielectric constant of some semiconductors at audiofrequencies”, *Phys. Rev.*, **83** (1951) 121–124.
 34. L.I. Rabinkin, L.I. Novikova, “Ferrites”, *Minsk: Izv. Acad. Nauk*, **16** (1960) 146.
 35. A.K. Jonscher, *Dielectric Relaxation in Solids*, Chelsea, Dielectric Press, London, UK, 1983.
 36. M.A. Ahamed, M.A. El Hiti, “Electrical and dielectric properties of $\text{Zn}_{0.8}\text{Co}_{0.2}\text{Fe}_2\text{O}_4$ ”, *J. Phys. III France*, **5** (1995) 775–781.
 37. M.A. Shaikh, S.S. Bellad, B.K. Chougule, “Temperature and frequency-dependent dielectric properties of Zn substituted Li-Mg ferrites”, *J. Magn. Magn. Mater.*, **195** (1999) 384–390.